MM Science Journal | www.mmscience.eu
ISSN 1803-1269 (Print) | ISSN 1805-0476 (On-line)
Special Issue | HSM 2019
15th International Conference on High Speed Machining
October 8-9, 2019, Prague, Czech Republic
DOI: 10.17973/MMSJ.2019_11_2019076

HSM2019-097

A NOVEL METHOD FOR THE CHARACTERIZATION OF DIAMOND WIRE TOPOGRAPHY AND ABRASIVE GRAIN GEOMETRIES

U. Pala[1]*, K. Wegener[1]

[1] Institute of Machine Tools and Manufacturing - IWF, ETH Zurich, Zurich, Switzerland

*Corresponding author; e-mail: palau@ethz.ch

Abstract
Diamond wire is a relatively new abrasive tool technology used in wire sawing of hard and brittle materials i.e. Si, SiC, sapphire or ceramics in general. Process characteristics such as the undeformed chip thickness, abrasive wear and material removal regime heavily depend on the wire properties. However, manufacturers only provide data on the abrasive grain size range, relative grain density and core wire diameter. A systematic investigation of the abrasive and wire properties is essential to develop a comparative understanding of the wire behavior as well as its influence on process outputs. Development of such a method requires the use of microscopy imaging tools and image processing algorithms. A proprietary wire analysis software is developed as a reference characterization method for the investigation of diamond wires in terms of abrasive grain geometry, distribution and density, grain protrusion and grain volume. The software applies statistical and geometrical analysis to characterize and compare diamond wires or investigate the wear progression at individual grain level. Additionally, the results can be used to model the stochastic nature of the wire, reproduce it; and to simulate the grain-workpiece interaction.

Keywords:
Diamond wire; Wire sawing; Diamond wire topography; Abrasive grain characterization; Grain geometry

1 INTRODUCTION

The expansion of the photovoltaic (PV) industry in the early 80's and its rapid growth in the 90's which was mainly driven by the increasing fuel costs [Chandra et al. 2014] have resulted in an increased attention to wafer production. The technology has evolved from inner/outer diameter saws to slurry-based multi-wire cutting and led to a 66% increase in the production efficiency at the time [Jester 2002], while increasing the wafer surface quality, reducing wafer thickness, improving cell efficiency and sustainability [Chung et al. 2014] [Chandra et al. 2014] [Jester 2002] [Kumar & Melkote 2018] [Yang et al. 2013].

The introduction of diamond wire sawing in mid-2000's led to the next revolution in the PV industry and subsequently dominated the sawing industry. Higher process efficiency and sustainability, increased wafer quality, and reduced kerf loss with diamond wires has led to a rapid technology shift. On top, only a few modifications are required on slurry-based wire saws to operate with diamond wires [Möller 2015], which reduced the upgrade costs significantly.

The diamond wire technology has enhanced as diamond wire sawing becomes the most common processing technology in wafering. Today, diamond wire sawing is being employed for the processing of mono crystal Si by 95% and multi crystal silicon by more than 50% in comparison to slurry-based sawing [ITRPV 2018]. On the other hand, wafering costs make up to 30% of the total production in PV and semiconductor industries and more than 90% of the solar cell production is dependent on machining of silicon [Möller 2019]. In diamond wire sawing, the wire length involved per cut is typically between 50-100 km [Sopori et al. 2016] and the wire cost is more than hundred times higher per km compared to steel wire employed in slurry-based sawing. The cost of the extensive wire lengths sum up to 20% of the total production costs [Luque & Hegedus 2011].

Diamond wires are composed of a steel wire core and diamond grains that are fixed on the surface by depositing filler metal (Nickel or nickel-cobalt alloys) by electroplating as shown in Fig. 1a. Typical wire core diameters are in the range of 80-140 µm with typical abrasive grain sizes in the range of 8-25 µm. Today down to 60 µm core diameter wires are used in production. A scanning electron microscope (SEM) image of an electroplated diamond wire is presented in Fig. 1b. The surface of the unworn wire and the diamond grains are completely or partly covered with the Ni-filler material that wears off as the wire wear propagates; leading to exposure of cutting edges of diamond grains.

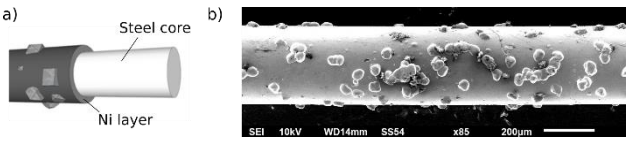

Fig. 1: (a) Steel core and Ni-filler layer of a diamond wire (b) SEM image of a new diamond wire.

The significant market share, high cost and high consumption as well as their high efficiency increase the attention in manufacturing and process related characteristics of diamond wires. In this aspect, it is crucial

to develop a detailed understanding of the abrasive grain geometries and positioning beyond the standard definitions for a more accurate evaluation and modeling of the sawing process.

2 LITERATURE REVIEW

Only little research work is available on the systematic, image based topography measurements of the diamond wire, however its fundamental similarities with the tools used in other abrasive processes such as grinding emerges the need to extend the literature review beyond the diamond wire technology to geometrically undefined cutting edges in general.

The description of micro- and macro- geometry of the abrasive tool is of high importance in understanding the kinematic interactions and developing the relevant process models. The macro-geometry of the tool is defined by its eccentricity and micro-geometry is defined by the grain size, geometry, strength and abrasive layer characteristics [Tönshoff et al. 2002] [Brinksmeier et al. 2006]. Determination of the abrasive tool topography is possible by direct and indirect measurements on the surface or statistical evaluation of the grain and tool properties. Several reviews are available in literature on the measurement of abrasive tool topographies and generation of topography models [Doman et al. 2006] [Verkerk 1977] [Tönshoff et al. 1992] [Lonardo et al 1996].

A number of classifications of the topography measurement methods are proposed such as grain counting, profilometry and taper print methods [Verkerk 1977]; contact and non-contact methods by [Lonardo et al 1996]. Non-contact methods can further be investigated in optical and non-optical; static, dynamic, and kinematic methods [Marinescu et al. 2007]. Dynamic methods depend on machining conditions and actual abrasive grains effective in cutting are measured; kinematic methods combine the process kinematics and distribution of the statically determined abrasive positions [Marinescu et al. 2007] [Bruecher 1996]. In the kinematic approach, trajectories of single grains are reproduced through geometric contact conditions and process parameters. Several techniques for the determination of grinding wheel topographies were stated by [Marinescu et al. 2007].

A three-dimensional contacting profilometery was used by [Blunt & Ebdon 1996], an automated non-contact 3D wheel scanning system was used by [Darafon et al. 2013], a 3D laser microscopy was employed by [Xie et al. 2011], 3D grain positions were derived from contact measurements by [Xie et al. 2008], optical profilometry was employed by [Inasaki 1996], SEM measurements of the grinding wheels were used by [Hwang et al. 2000], imprints of the wheel on a polished lead sample were used by [Hecker et al. 2003], and photoelectric measurements are used by [Brinksmeier & Werner 1992].

The lack of determined grain shapes of crushed diamonds limits grain geometry modeling. Studies on diamond wire sawing require broad assumptions of the abrasive grain geometries for the development of relevant process models. Conical grain shapes are mainly considered with a normal distribution for the grain protrusion and fixed tip angles [Chung 2012] [Chung et al. 2014] [Liu et al. 2016] [Wu et al. 2014] [Wang et al. 2017]. For the measurement of diamond wires, Lee [Lee et al. 2015] introduced a quick measurement system for measuring the wire contour to determine the grain protrusion over the wire.

The Wire Analysis Software (WAS) is developed to provide a software tool to analyze diamond wires in terms of grain geometries, cutting edge distribution and density and other wire and abrasive grain properties i.e. chipping space, grain protrusion, volume or material ratio. Development of such a method requires the use of microscopy imaging tools as well as image processing algorithms. It is possible to measure and evaluate samples from different sections of the diamond wire with the WAS. It determines a wire reference level on which the topographic elements are identified. Through the application of size and ratio filters, a statistical analysis of the output data is provided.

3 MEASUREMENT AND PRE-PROCESSING OF THE WIRE SAMPLES

The software employs optical images taken by an Alicona 3D Microscope (Alicona IFM) and the cylinder mantle surface is folded up as shown in Fig. 2, to give a reference plane, using the form removal software of the Alicona IFM, confirming ISO Standards [ISO5426 2012] [ISO1101 2017]. The form removal process operates at a maximum standard deviation of less than 0.2 µm and a mean standard deviation of less than 0.03 µm in 95% confidence interval.

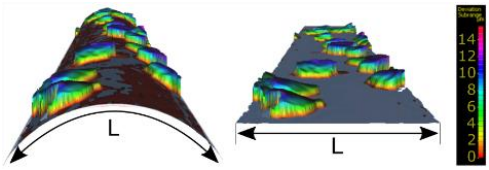

Fig. 2: Comparison of cylindrical and form removed surfaces.

The image is then transformed into a threshold image of 256 grayscale levels defined by the grain protrusion height, where 0 is the zero level (black) and 255 is the top level (white) (Fig. 3). The resolution depends on the protrusion of the highest grain h_g^{max} of the sample, where 20 µm is typical for the investigated diamond wires in this work. The vertical resolution of WAS is then derived to be:

$$\delta_z = h_g^{max}/256 \quad (1)$$

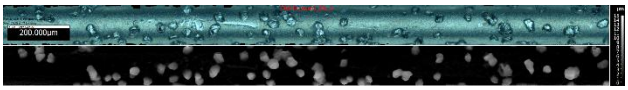

Fig. 3: Transformation of the wire surface topography to grayscale.

3.1 Details of the Analysis

The WAS processing flowchart is presented in Fig. 4. Several wire sections of the same wire types are used as individual inputs to determine the wire and abrasive grain characteristics. Processing of a sample starts with the thresholding step. After, a size filter of A_{lim}=250 px is applied to the first threshold level using the MATLAB function *bwareaopen*. The value of A_{lim} is in pixels and depends on the lens used for imaging (In this study, Alicona IFM 20X lens is employed). It is evaluated that in the first threshold layer, surface elements below A_{lim} can only be the result of the Ni filler and not abrasives, hence should be removed. The positions and size of the elements are deleted from the rest of the sample layers. Later, for each layer, the function *bwconncomp* is used to determine the surface elements with 8-point connectivity. Following, the *regionprobs* function is applied to extract the areas and center positions of the topographic elements.

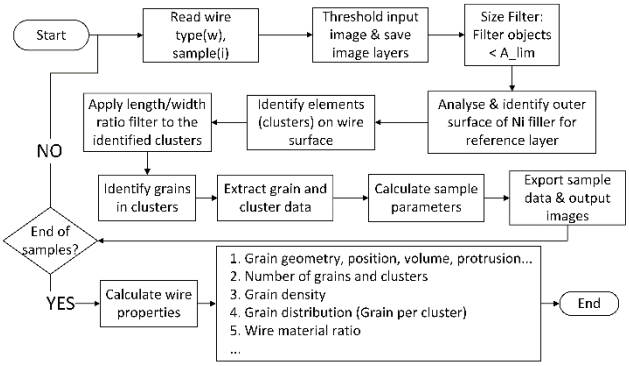

Fig. 4: The WAS algorithm process flow.

Fig. 5 introduces the parameters of abrasive grain characterization by the WAS. The base frame area is measured at the outer surface, corresponding to the outer layer of the Ni-filler material which is denoted as the zero level. The grain length l_g is along the grain width w_g is orthogonal to the wire length. The grain base area A_b is measured at the same level. Grain protrusion h_g is measured from the zero level to the maximum protrusion height and the grain volume V_g is the volume enveloped by the grain length l_g, grain width w_g and grain protrusion height h_g. The grain volume V_g is calculated by summing up the individual grain layer areas at each threshold layer.

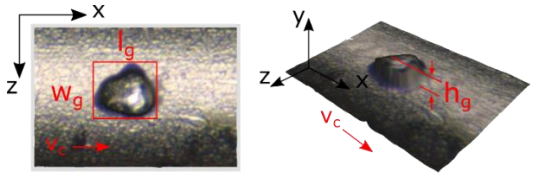

Fig. 5: Grain geometry parameters measured by the WAS.

3.2 Determination of the Reference Layer

Individual grains are required be distinguished from the other surface elements that are the result of Ni-filler material deposition (See Layer 1 in Fig. 8). This is possible at a height, where grains are the only visible elements on the surface layer. Moreover, this surface height varies for different sections of the wires. Hence, determination of individual reference layers for each wire sample is essential. After the grains are identified at the reference layer, the grain positions and cross-sections are saved and grains are evaluated through the layers above and below the reference layer.

For the calculation of the reference layer, bounding boxes are plotted around each and every surface element on each layer, at their maximum points along and orthogonal to the wire length as shown in Fig. 6a. The bounding boxes are separately shown in Fig. 6b. The box areas are analyzed for their 8-point connectivity and the total area covered are saved for each layer, which is called the superimposed layer surface and is shown in Fig. 6c.

Fig. 6: (a) Bounding boxes plotted around surface elements at their maximum points along and orthogonal to the wire length (b) Frames around the elements (c) Superimposed bounding box areas.

The difference between the sum of individual bounding areas and the superimposed area is calculated for each layer as:

$$A^l_{diff} = A^l_{simp} - \sum_{i=1}^{n} A^l_i \qquad (2)$$

Where for layer l, A^l_{diff} is the difference between the superimposed area A^l_{simp} and the sum of individual bounding box areas A^l_i, i is the individual surface element and n is total number of the surface elements. It is suggested that layer l is the reference layer if and only if:

$$A^{l-1}_{diff} < 0 \wedge A^l_{diff} > 0 \qquad (3)$$

A^l_{diff} for the first 64 layers of the analyzed sample are plotted in Fig. 7. According to Eq. (3), Layer 7 which corresponds to the vertical height of 0.547 µm (See Eq. (1)), measured from the outer diameter of the wire surface is determined as the reference layer for this wire sample.

The difference between the superimposed areas and the individual grain areas is negative before the reference layer, since the superimposed area is smaller due to overlapping (See Figure 6a and b). In the layers higher than the reference layer, the difference will be positive, since the bounding box areas are always bigger than the individual grain areas. But over the reference layer, the difference between these two would be stable as the bounding boxes are distant enough so that the difference between the grain areas and bounding box areas at each layer are changing at the same rate (See Figure 8, Layer 7).

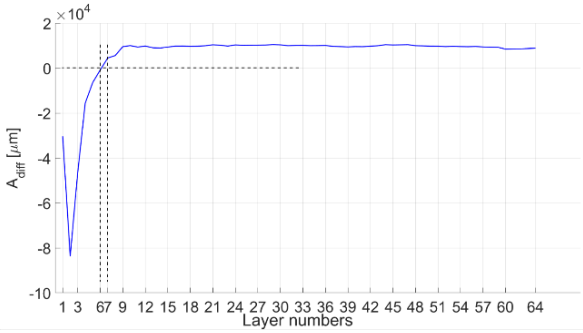

Fig. 7: Plot of the difference between the bounding boxes and actual areas of grains in layers 0 to 64.

Fig. 8 shows Layers 1, 6 and 7 of the same wire sample in Fig. 7, where the surface topography of the layer is given on top and plotted bounding boxes on the same layer is given below, for each layer.

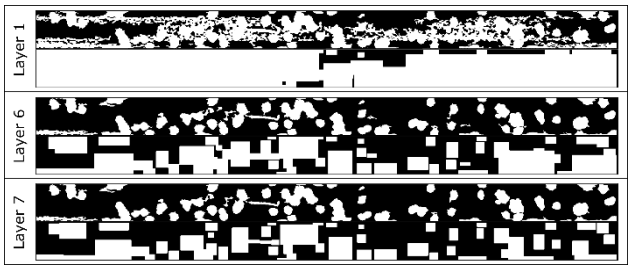

Fig. 8: Layers 1, 6 and 7 from Asahi 12-25 high concentration diamond wire. Actual wire layer is given on top and same layer with bounding boxes is given below, for each layer.

3.3 Analysis of the Topographic Elements

The topographic elements on the reference layer are identified and numbered. The aspect ratios (l_g/w_g) of the identified elements are calculated and further, the upper and lower control limits of one standard deviation are

applied as shown in Fig. 9. The topographic elements between these limits are then assigned as the abrasive grains.

Fig. 9: The length/width ratio filter with upper and lower control limits. Base areas that are measured at the reference layer are shown and topographic elements that are outside the upper and lower control limits are not included in the analysis.

Identified grain base areas measured at the reference layer of the wire sample are given in Fig. 10. It can be seen that the surface elements can be divided into two categories as individual grains and two or more grains that are a part of the same, larger surface structures.

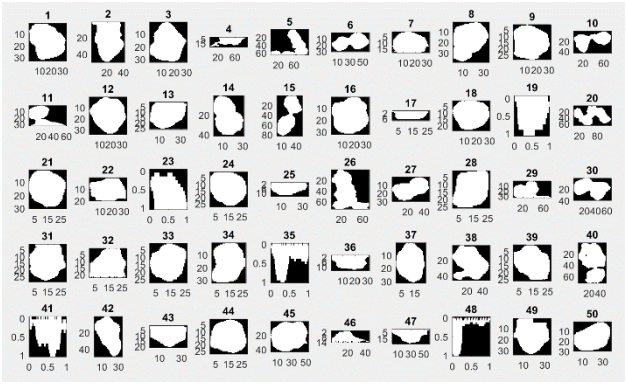

Fig. 10: Identified cluster base areas at the reference layer.

Such an aggregation of grains is defined as a cluster. They are the result of a nonhomogeneous distribution of diamonds on the wire surface where the distances between the diamonds are close enough and usually filled with the Ni-filler material. The available chip space is too small and thus clusters are sources of loading risk and premature failure of the abrasive layer. Formation of clusters may affect the cutting ability since grains with highest protrusion in the cluster is kinematically active, hence leaving the other grains in the proximity inactive. Visualization of the cluster formations is shown in Fig. 11.

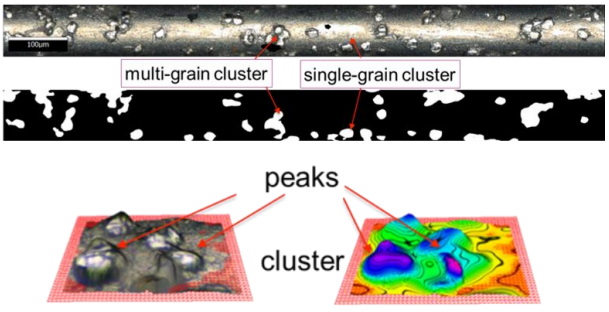

Fig. 11: Comparison of single grains and clustered on the diamond wire surface.

Fig. 12 explains how the cutting edges or grains can be determined in a cluster structure. As the area of the bounding box for each topographic structure is defined on the reference level and stays constant through the layers, grains can be counted on each topographic element on the wire surface and their protrusion height can be determined.

Fig. 12: Horizontal cross-sections of the same cluster structure at different heights from layer 30 to layer 140, revealing the peak of each grain in the cluster structure thus identifying individual grains.

3.4 Validation

Validation of the WAS outputs are done for Asahi 12-25 120 µm core standard concentration wire. Fig. 13 presents the comparison of the WAS analysis results and the results of measurement conducted with Alicona IFM software concerning the distribution of grain protrusions. The abrasive grains show a normal distribution around of the same mean height and it can be concluded that the WAS is able to determine the distribution characteristics and maximum grain protrusion heights of the analyzed wires.

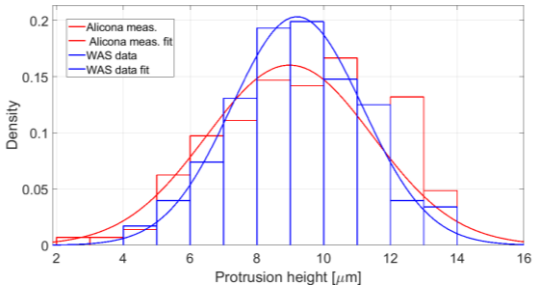

Fig. 13: Distribution data and curve fits of grain protrusion heights of 4 samples of Asahi 12-25 120 µm core standard concentration wire measured by WAS and Alicona IFM software.

3.5 Comparison of Diamond Wires

Five wires manufactured by Asahi and DMT (Asahi 10-20, HC, 120 / Asahi 10-20, SC, 120 / Asahi 8-16, HC, 120 / Asahi 8-16, SC, 120 / DMT 8-16, SC, 100) with varying diamond densities and grain sizes are analyzed with the WAS. The results are tabulated in Tab. 1. The denotation of the wire names is given as: Manufacturer, grain size range [µm], grain density (HC: High concentration / SC: Standard concentration, core wire diameter [µm]. High number of grain samples of around 1000 grains from each wire type are measured.

The WAS successfully identified higher grain densities for HC wires and higher grain protrusions for wires with bigger grains. The analysis results indicate that wires with higher grain densities (HC) possess higher number of cluster structures, indicated in the cluster density values. Additionally, for the HC wires, the average number of grains in clusters is higher compared to the SC wires, which is likely to result in smaller grain-bond interface and lower retention forces. Moreover the average protrusion of the clustered grains (clusters) are higher than the average grain protrusion. In the wire sawing process, the abrasives with the highest protrusion on the wire are subject to the initial load. Hence, it can be suggested that the wires with higher grain concentration are more likely to suffer from premature pull-outs due to lower retention forces and/or macro grain break-outs at the initial phase of the sawing process, leading to reduced surface quality.

Tab. 1: Characterization of new diamond wires.

	(a) Asahi 10-20 HC Ø120	(b) Asahi 10-20 SC Ø120	(c) Asahi 8-16 HC Ø120	(d) Asahi 8-16 SC Ø120	(e) DMT 8-16 SC Ø100
Number of grains	1315	1421	1068	696	1287
Grain protrusion [µm]	9.39 ± 3.75	8.50 ± 4.53	8.02 ± 3.30	6.09 ± 2.47	6.93 ± 2.82
Cluster protrusion [µm]	10.21 ± 3.47	9.17 ± 4.32	8.14 ± 3.09	6.45 ± 2.42	7.08 ± 2.75
Grain per cluster	1.80 ± 0.94	1.68 ± 0.77	1.59 ± 0.78	1.44 ± 0.76	1.64 ± 0.85
Grain density [grains/µm²]	4.63e-4 ± 1.1e-4	4.13e-4 ± 1.6e-4	7.4e-4 ± 0.69e-4	4.81e-4 ± 1.3e-4	4.81e-4 ± 1.0e-4
Cluster density [clusters/µm²]	3.01e-4 ± 0.44e-4	2.87e-4 ± 0.84e-4	5.42e-4 ± 0.32e-4	3.89e-4 ± 0.78e-4	3.50e-4 ± 0.71e-4
Cluster vol. [µm³]	2748.41 ± 328.9	2581.61 ± 282.9	1454.24 ± 243.0	926.13 ± 106.9	1757.13 ± 92.6

Tab. 2: Evaluation of the diamond wire wear of Asahi 10-20 SC Ø120.

	New Wire	6.54 cm³/m	8.10 cm³/m
Number of grains	1421	1458	1481
Grain protrusion [µm]	8.50 ± 4.53	4.05 ± 2.30	3.00 ± 2.41
Cluster protrusion [µm]	9.17 ± 4.32	4.12 ± 2.33	2.83 ± 2.52
Grain per cluster	1.68 ± 0.77	1.60 ± 0.87	1.42 ± 0.71
Grain density [grains/µm²]	4.13e-4 ± 1.5e-4	4.62e-4 ± 1.9e-4	5.21e-4 ± 2.88e-4
Cluster vol. [µm³]	2581.61 ± 282.37	1328.14 ± 142.4	918.18 ± 87.5

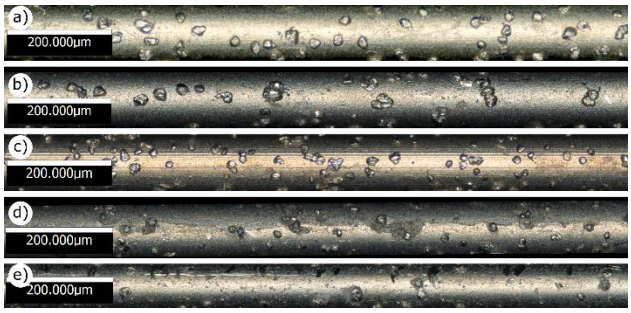

Fig. 14: Wire samples measured with Alicona IFM at 20X magnification and characterized with the WAS. The letter notation is as indicated in Table 1.

3.6 Evaluation of the Wire Wear

Further, the wear states of Asahi 10-20 SC Ø120 diamond wire used in sawing of monocrystalline silicon on a Meyer Burger DW288 multi-wire saw at the wire speed of 25 m/s and the feed rate of 1.5 mm/min are investigated with the WAS. Three stages of wire wear are measured as the new wire, 6.54 cm³/m and 8.10 cm³/m of specific material removal rates, which are expressed as the total material removal volume per unit wire length consumed. The average values are tabulated in Tab. ***2*** and samples wire sections are given in Fig. 15.

The average grain and cluster protrusions reduce as wear propagates. Moreover, the number of grains per cluster is reducing and the grain density is increasing with the increasing wear, which is likely due to the wear of the bonding material that fills the voids in cluster structures. This results in a decrease in the number of grains per cluster and increase in the grain density. Additionally, it is measured that the average cluster volume is decreasing which also points out the clusters are breaking out with wear progress. Similar results were achieved by Pala [Pala et al. 2018] on the diamond wire wear experiments conducted on a quick-wire wear experiment setup.

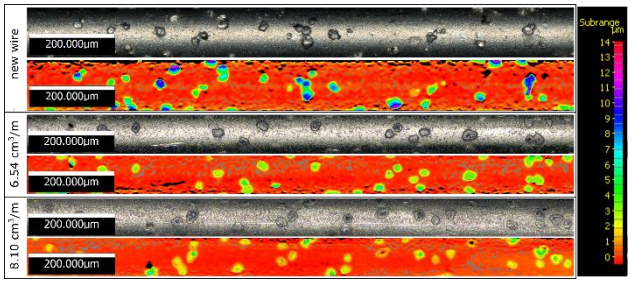

Fig. 15: Three wear stages of Asahi 10-20 SC Ø120 wires. Real color images are on top and color-coded images are below each sample.

4 SUMMARY

The presented research introduces the Wire Analysis Software, developed for the evaluation of diamond wire topographies and abrasive grains, through the application of 3D confocal microscopy and image processing algorithms. For the application, characterization of new diamond wires with the WAS is presented. The quantitative measurements comply with manufacturers' definitions. The clustering property of diamond wires is introduced and determined in several wire types, and also cluster evolution over wear propagation is discussed. Changes in wire topography with wire wear is measured and discussed.

The software is able to specify a reference layer where the surface elements are distinguished, applies size and ratio filters to determine the abrasive geometry, distribution (defined by number and size of clusters), density, protrusion and volume. The software provides the possibility for the

comparison of topographic properties of diamond wires from different manufacturers and further can be used to evaluate individual grain wear, since individual grains are located and numbered. It also provides a useful basis for the modeling of diamond wires and wire sawing process. To the author's knowledge, there is no software available for the characterization of diamond wires to this level. The software can also be used for several other abrasive tool analysis as it is fast, standardized and able to compare individual topographic elements over lifetime.

5 REFERENCES

[Blunt & Ebdon 1996] Blunt, L. and Ebdon, S., The application of three-dimensional surface measurement techniques to characterizing grinding wheel topography. International Journal of Machine Tools and Manufacture, 1996. Vol.36, No.11, pp 1207-1226.

[Brinksmeier et al. 2006] Brinksmeier, E. et al. Advances in Modeling and Simulation of Grinding Processes. CIRP Annals - Manufacturing Technology, 2006. Vol.55, No.2, pp 667-696.

[Brinksmeier & Werner 1992] Brinksmeier, E. and Werner, F., Monitoring of Grinding Wheel Wear. CIRP Annals, 1992, Vol.41, No.1, pp 373-376.

[Bruecher 1996] Bruecher, T., Kühlschmierung beim Schleifen keramischer Werkstoffe, Berlin: Technische Universität Berlin, 1996.

[Chandra et al. 2014] Chandra, A., Anderson, G., Melkote, S., Gao, W., Haitjema, H. and Wegener, K., Role of surfaces and interfaces in solar cell manufacturing. CIRP Annals, 2014. Vol.63, No.2, pp 797-819.

[Chung 2012] Chung, C. H., Abrasive Distribution of the Fixed Diamond Wire in Wire Sawing Process. Advanced Materials Research, 2012. Vol.579, pp. 145-152.

[Chung et al. 2014] Chung, C., Tsay, G. D. and Tsai, M.-H., Distribution of diamond grains in fixed abrasive wire sawing process. The International Journal of Advanced Manufacturing Technology, 2014. Vol.73, No.9, pp 1485-1494.

[Darafon et al. 2013] Darafon, A., Warkentin, A. and Bauer, R., Characterization of grinding wheel topography using a white chromatic sensor, International Journal of Machine Tools and Manufacture, 2013. Vol.70, pp 22-31.

[Doman et al. 2006] Doman, D. A., Warkentin, A. and Bauer, R., A survey of recent grinding wheel topography models. International Journal of Machine Tools and Manufacture, 2006. Vol.46, No.3, pp 343-352.

[Hecker et al. 2003] Hecker, R. L., Ramoneda, I. M. and Liang, S. Y., Analysis of wheel topography and grit force for grinding process modeling. Journal of Manufacturing Processes, 2003. Vol.5, No.1, pp 13-23.

[Hwang et al. 2000] Hwang, T. W., Evans, C. J. and Malkin, S., High Speed Grinding of Silicon Nitride With Electroplated Diamond Wheels, Part 2: Wheel Topography and Grinding Mechanisms. Journal of Manufacturing Science and Engineering, 2000. Vol.122, No.1, pp 42-50.

[Inasaki 1996] Inasaki, I., Grinding Process Simulation Based on the Wheel Topography Measurement. CIRP Annals, 1996. Vol.45, No.1, pp 347-350.

[ISO1101 2017] ISO 1101, Geometrical product specifications (GPS) - Geometrical tolerancing: Tolerances of form, orientation, location and run-out. 2017.

[ISO5426 2012] ISO 5436, Geometrical product specifications (GPS) - Surface texture: Profile method; Measurement standards -- Part 2: Software measurement standards, 2012.

[ITRPV 2018] ITRPV, International Technology Roadmap for Photovoltaic, 2018.

[Jester 2002] Jester, T. L., Crystalline silicon manufacturing progress. Progress in Photovoltaics: Research and Applications, 2002. Vol.10, No.2, pp 99-106.

[Kumar & Melkote 2018] Kumar, A. and Melkote, S. N., Diamond Wire Sawing of Solar Silicon Wafers: A Sustainable Manufacturing Alternative to Loose Abrasive Slurry Sawing. Procedia Manufacturing, 2018. Vol.21, pp 549-566.

[Lee et al. 2015] Lee, S., Kim, H., Kim, D. and Park, C., Investigation on diamond wire break-in and its effects on cutting performance in multi-wire sawing. The International Journal of Advanced Manufacturing Technology, 2015. Vol.87, No.1, pp 1-8.

[Liu et al. 2016] Liu, T., Ge, P., Gao, Y. and Bi, W., Depth of cut for single abrasive and cutting force in resin bonded diamond wire sawing. International Journal of Advanced Manufacturing Technology, 2016. pp 1-11.

[Lonardo et al. 1996] Lonardo, P. M., Trumpold, H. and De Chiffre, L., Progress in 3D Surface Microtopography Characterization. CIRP Annals, 1996. Vol.45, No.2, pp 589-598.

[Luque & Hegedus 2011] Luque, A. and Hegedus, S., Handbook of Photovoltaic Science and Engineering, 2011. Second ed. United Kingdom: John Wiley & Sons.

[Marinescu 2007] Marinescu, I. D. et al., Handbook of Machining with Grinding Wheels, 2007. CRC Press.

[Möller 2015] Möller, H. J., Wafer Processing. In: Handbook of Crystal Growth, 2015. Boston: Elsevier, pp 715-755.

[Möller 2019] Möller, H. J., Wafer Processing. In: Handbook of Crystal Growth, 2019. Berlin, Heidelberg: Springer, pp 1-41.

[Pala et al. 2018] Pala, U., Süssmaier, S., Kuster, F., Wegener, K., Experimental investigation of tool wear in electroplated diamond wire sawing of silicon, Procedia CIRP, 2018. Vol.77, pp.371-374.

[Sopori et al. 2016] Sopori, B., Devayajanam, S. and Basnyat, P., Surface characteristics and damage distributions of diamond wire sawn wafers for silicon solar cells. AIMS Materials Science, 2016, Vol.3, No.2, pp 669-685.

[Tönshoff et al. 1992] Tönshoff, H. K., Peters, J., Inasaki, I. and Paul, T., Modelling and Simulation of Grinding Processes. CIRP Annals - Manufacturing Technology, 1992, Vol.41, No.2, pp 677-688.

[Tönshoff et al. 2002] Tönshoff, H. K., Friemuth, T. and Becker, J. C., Process Monitoring in Grinding. CIRP Annals, 2002, Vol.51, No.2, pp 551-571.

[Verkerk 1977] Verkerk, J., Final Report Concerning CIRP Cooperative Work on the Characterization of Grinding Wheel Topography, Annals of the CIRP, 1977. Vol.26, No.2.

[Wang et al. 2017] Wang, P., Ge, P., Gao, Y. and Bi, W., Prediction of sawing force for single-crystal silicon carbide with fixed abrasive diamond wire saw. Materials Science in Semiconductor Processing, 2017. Vol.63, pp 25-32.

[Wu et al. 2016] Wu, C., Jiang, Z., Fan, W. and Chen, L., Finite element analysis of multi-wire saw silicon rods with consolidated abrasive diamonds. The International Journal of Advanced Manufacturing Technology, 2016. pp 1-8.

[Xie et al. 2008] Xie, J., Xu, J., Tang, Y. and Tamaki, J., 3D graphical evaluation of micron-scale protrusion topography of diamond grinding wheel. International Journal of Machine Tools and Manufacture, 2008. Vol.48, No.11, pp 1254-1260.

[Xie et al. 2011] Xie, J. et al., 3D laser investigation on micron-scale grain protrusion topography of truncated diamond grinding wheel for precision grinding performance. International Journal of Machine Tools and Manufacture, 2011. Vol.51, No.5, pp 411-419.

[Yang et al. 2013] Yang, C., Wu, H., Melkote, S. and Danyluk, S., Comparative Analysis of Fracture Strength of Slurry and Diamond Wire Sawn Multicrystalline Silicon Solar Wafers. Advanced Engineering Materials, 2013. Vol.15, No.5, pp 358-365.